Peer-reviewed version available at *Sensors* **2018**, *18*, 4201; doi:10.3390/s18124201

Article

Suitable Combination of Direct Intensity Modulation and Spreading Sequence for LIDAR with Pulse Coding

Gunzung Kim and Yongwan Park *

Department of Information and Communication Engineering, Yeungnam University, 280 Daehak-Ro, Gyeongsan, Gyeongbuk 38541, Republic of Korea; gzkim@yu.ac.kr

* Correspondence: ywpark@yu.ac.kr; Tel.: +82-53-810-3942

Abstract: In the coded pulse scanning light detection and ranging (LIDAR) system, the number of laser pulses used at a given measurement point changes depending on the modulation and the method of spreading used in optical code-division multiple access (OCDMA). The number of laser pulses determines the pulse width, output power, and duration of the pulse transmission of a measurement point. These parameters determine the maximum measurement distance of the laser and the number of measurement points that can be employed per second. In this paper, we suggest possible combinations of modulation and spreading technology that can be used for OCDMA, evaluate the performance and characteristics of them, and study optimal combinations according to varying operating environments.

Keywords: LIDAR; time-of-flight; IM/DD OCDMA; free-space optical communication; modulation; spreading code

Key Contribution: We suggest possible combinations of modulation and spreading technology that can be used for OCDMA, evaluate the performance and characteristics of them, and study optimal combinations according to varying operating environments.

1. Introduction

Pulse scanning light detection and ranging (LIDAR) measures the distance to a given object using a time-of-flight (ToF) technique that calculates the time required for a pulse to transmit to and reflect off the object [1–6]. The distance image of the surroundings can be generated with excellent angular resolution and is used to determine the area that can be traveled while mounted on an autonomous vehicle or an autonomous mobile robot. Many factors determine the operating characteristics of pulse scanning LIDAR and can be divided into characteristics of the transmission and generation of a pulse, and those of the reception of a reflected pulse [3,7,8]. In the transmitter, the pulse scanning LIDAR determines the wavelength of the laser as well as pulse width, interval, and peak power [9]. In the receiver, it determines the size of the receiving aperture, and uses a photodetector, a pulse detection method, the threshold-to-noise ratio (TNR), and a range estimation method [10–13]. The characteristics used to generate pulses in the transmitter are limited by the maximum permissible exposure (MPE) to comply with eye safety standards [14]. The most critical parameter that determines the maximum measurement distance in LIDAR is the pulse peak power of the transmitter and the TNR of the receiver. As the strength of the received signal is proportional to the peak power of the pulse and inversely proportional to the square of the measured distance, the higher the pulse peak power and the lower the TNR, the greater the distance that can be measured. Thus, if the characteristics of one parameter are improved, the characteristics of the other parameters worsen [9]. Depending on the primary purpose of LIDAR, one or two of parameters are used as characteristics of preference, and the remaining are rendered MPE compliant.

Peer-reviewed version available at Sensors 2018, 18, 4201; doi:10.3390/s18124201

Some studies have focused on solving the range ambiguity of pulse scanning LIDAR by used pulse coding to avoid crosstalk [15–19] or mutual interference that occurs when two or more LIDARs simultaneously operate [18–20]. Such LIDARs measure distances using multiple pulses generated by random sequences [15–17] or specially designed codes [18–20], rather than one pulse per measurement point. Even if multiple pulses are used, the parameters that determine the characteristics of the transmitter in the conventional pulse scanning scheme are maintained. To comply with eye safety standards, the pulse peak power is distributed across several pulses so that the energy allocated to a pulse decreases in inverse proportion to the number of pulses, and the time required to transmit pulses at a given measurement point is proportional to the number of pulses [18–20]. The use of multiple pulses also enhances the accuracy of the distance measurement [19].

In LIDAR with pulse coding [18,19], the number of pulses used at a measurement point is determined by the modulation method and the spreading code method, as illustrated in Figure 1. The optical channel differs significantly from radio frequency (RF) channels. Unlike RF systems, where the amplitude, frequency, and phase of the carrier signal are modulated, the intensity of the optical carrier is modulated in optical systems. In an optical wireless communication system using unipolar signaling, the numbers and positions of the pulses to be transmitted and empty slots are determined by the modulation and spreading code methods used [21–25]. To accurately demodulate and despread the signal at the receiver of the code pulse LIDAR, both the numbers and the positions of the pulses and the empty slots are used. In a unipolar optical communication system, on–off keying (OOK), pulse position modulation (PPM), differential PPM (DPPM), multipulse PPM (MPPM), digital pulse interval modulation (DPIM), and dual-header pulse interval modulation (DH-PIM) are widely used as modulation techniques, and prime code (PC) and optical orthogonal code (OOC) are widely used as spreading code techniques [21–23]. The number of pulses, pulse peak power, average signal-to-noise ratio (SNR), maximum measurable distance, accuracy and precision of the measured distance, and packet error rate (PER) vary depending on the combination of modulation scheme and spreading code scheme used. In this paper, we investigate the characteristics of various modulations and spreading code methods that can be used for LIDAR with pulse coding and compare various characteristics of LIDAR according to the combinations.

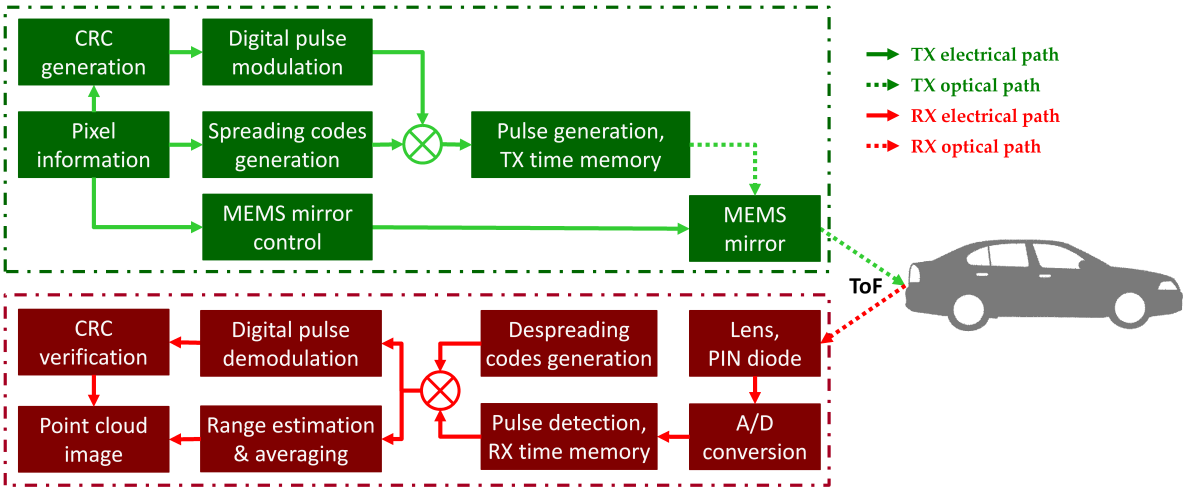

Figure 1. Overall architecture and operation flow of the proposed scanning light detection and ranging (LIDAR) system

Preprints (www.preprints.org) | NOT PEER-REVIEWED | Posted: 5 October 2018 doi:10.20944/preprints201810.0108.v1

Peer-reviewed version available at Sensors 2018, 18, 4201; doi:10.3390/s18124201

2. Digital modulation and spreading codes

2.1. Digital pulse modulation schemes

Because the average optical power of LIDAR is constrained, it is useful to determine a modulation scheme that can provide the requisite bandwidth and use power efficiently. Many digital modulation schemes have been proposed for use in optical wireless communication systems. Given the requirements, the performance of a communication system depends on how the information is represented in the modulation scheme. Types of modulation are thus the critical determinant of system design. In digital modulation schemes, information is embedded in both mark and space periods, and encoding is a term in discrete time slots. Each discrete amplitude of a modulated signal appears by varying the characteristics of the pulse at a discrete time. Such time characteristics as pulse position, width, and spacing are modulated using the instantaneous modulation signal but a constant sampling frequency is sustained. The OOK provides higher bandwidth efficiency but poor optical power performance. Digital pulse time modulation techniques such as PPM, DPPM, MPPM, DPIM, and DH-PIM are recognized as block codes through the OOK, which provides a balance between bandwidth and optical power efficiency [23]. Digital modulation schemes can be divided into two main categories: isochronous and anisochronous. In an isochronous mode, the length of the symbol is fixed; in the anisochronous mode, the length of the symbol is variable. The OOK, PPM, and MPPM are isochronous, whereas the DPPM, DPIM, and DH-PIM are anisochronous. An illustration of the overall conversion method and the time waveforms of modulation techniques with fixed pulse width that are discussed–the OOK, PPM, DPPM, MPPM, DPIM, and DH-PIM–are shown in Figure 2.

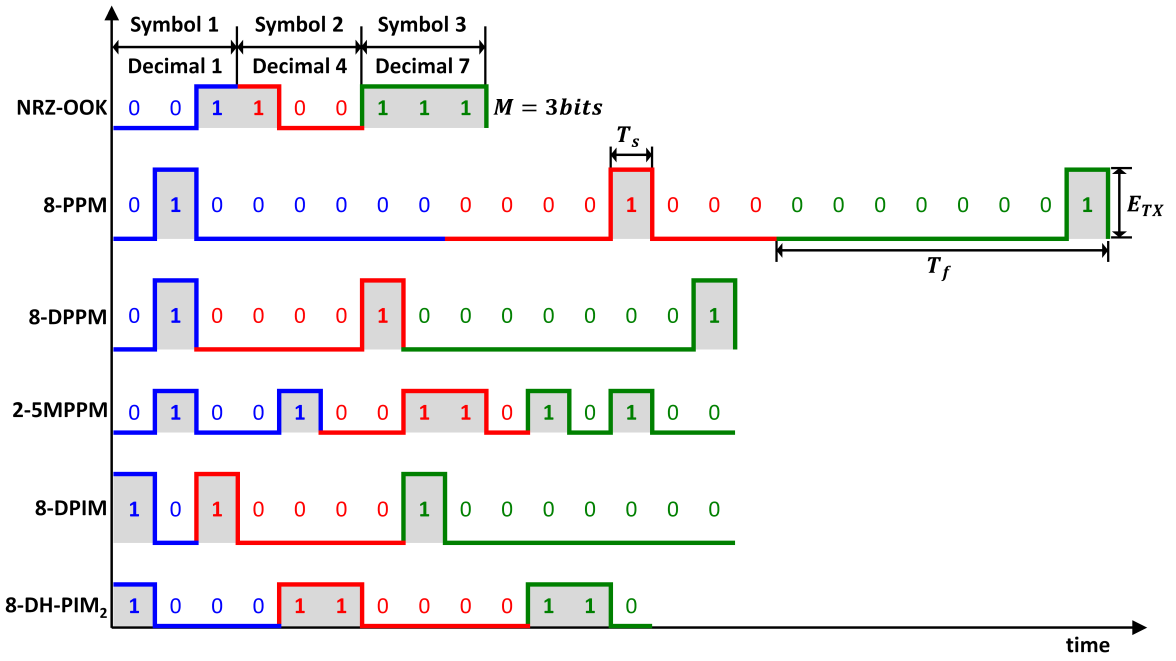

Figure 2. Time waveforms for OOJ, PPM, DPPM, MPPM, DPIM, and DH-PIM signals. E_{TX} is the pulse peak power, T_f is the block duration, and T_s is the time slot duration.

The OOK is the predominant pulse modulation format in optical wireless communication systems. It uses the simple method of amplitude-shift keying (ASK) modulation that represents digital data depending on the presence of an optical pulse [23,26–28]. In its simplest form, the presence of a pulse for a particular bit duration is represented by "1", and its absence for the same bit duration is represented by "0." The OOK can be either return to zero (RZ) or non-return to zero (NRZ). In

Peer-reviewed version available at Sensors 2018, 18, 4201; doi:10.3390/s18124201

NRZ-OOK, the pulses fill the entire bit duration; and in RZ-OOK, they occupy a particular portion of the bit duration. Owing to the relatively wide pulse, NRZ-OOK has higher bandwidth efficiency but lower power efficiency than RZ-OOK. In the OOK, symbols are displayed as amplitude pulse groups. A combination of an M-bit input block with symbols for on or off can represent $L = 2^M$ unique combinations. Three significant advantages of the OOK are that it provides a high SNR, low distortion performance, and superior system linearity, all of which are independent of channel quality.

In the PPM, each bit of an M-bit input block is mapped to one of $L = 2^M$ possible symbols [23,26–30]. A frame consists of a pulse that occupies a slot, and the remaining slots have no pulse. Therefore, the information is displayed as pulse position within the same symbol as the decimal value of the M-bit input block. Because the PPM requires both slot and symbol synchronization at the receiver to demodulate the signal, it delivers impressive optical power performance but at the cost of bandwidth and circuit simplicity.

The MPPM is a generalization of the PPM that allows more than one pulse per symbol. Moreover, w-pulse n-slot MPPM has (nw) unique symbols that correspond to filling n slots with w pulses in a frame [26,28–36]. As the level of coding increases, the number of PPM slots and the required transmission bandwidth both increase exponentially. To overcome these limitations, the MPPM was introduced as a way to improve the bandwidth utilization of the PPM. This approach reduces the bandwidth to half of that in the traditional PPM at the same transmission efficiency. That is, a single frame can carry information of size $\log_2(nw)$ bits. On the contrary, for the PPM, this rate is $\log_2 L$ bits. The amount of information that the MPPM can transfer increases with the number of pulses in the fixed-length frame. The disadvantage is that if one or more of these pulses are erroneous, the frame is incorrectly demodulated. Therefore, too many source bits are affected. The MPPM provides information capacity twice as poor as that of the PPM and is inferior to it in terms of error performance.

In the DPPM, $M = \log_2 L$-bit input block maps to one of L unique DPPM symbols, including a pulse and $L - 1$ empty slots [26–28,30,37,38]. The DPPM symbol is derived from the corresponding PPM symbol by removing all empty slots following the pulse, thus reducing the average symbol length and increasing bandwidth efficiency. The DPPM indicates its own symbol synchronization when all symbols end with a pulse. For a long sequence of zeros, there may be a slot synchronization problem that can be handled using a guard slot (GS) immediately after the pulse is removed. The DPPM improves bandwidth and power efficiency over the PPM for fixed average bit rate and fixed available bandwidth.

The DPIM has built-in symbol synchronization that improves bandwidth efficiency and data speed compared with the PPM, and power efficiency compared with the OOK [23,26–28,30]. The waveform of the DPIM is similar to that of the DPPM except that the variable frame length and the pulse are located at the beginning of the frame. In the DPIM, each symbol starts with a pulse of short duration after the optional GS followed by the number of empty time slots, which is determined by the decimal value of the bit input block. In other words, a symbol is represented by a discrete interval between consecutive pulses belonging to two consecutive frames. The GS consists of zero or more empty slots and is vital to avoiding continuous pulses when the input symbol is zero. The frame length of the DPIM may vary depending on the bit input block. In the DPIM, an M-bit input block of duration T_f (where $T_f = MT_b$, T_b is an equivalent binary bit period) is represented by a single pulse located in one of the $L = 2^M$ time slots. The speeds of the DPIM and DPPM slots increase exponentially with OOK bit rates as bit resolution increases. If two systems are included in the GS, this increase is even greater. As the slot frequency increases, bandwidth requirements also increase.

In DH-PIM, a symbol consists of two sections: a heading that starts a symbol and an ending information section. The nth symbol $S_n(h_n, d_n)$ starts with the header h_n of the duration $T_h = (\alpha + 1)T_s$ and ends with the sequence of d_n empty slots, where $\alpha > 0$ is an integer [23,26,27]. Depending on the most significant bit (MSB) of the input block, two headers are considered, H_1 and H_2, corresponding to $MSB = 0$ and $MSB = 1$, respectively. H_1 and H_2 have pulses of $0.5\alpha T_s$ and αT_s, respectively. Each pulse is followed by a GS of appropriate length T_g $<=$ *equation*; The value of dn $<=$ *equation* is

Peer-reviewed version available at Sensors 2018, 18, 4201; doi:10.3390/s18124201

the decimal value of the input block if the symbol starts with H_1. If the symbol starts with H_2, it is the decimal value of the 1's complement of the input code word. The header pulses play the dual role of symbol initiation and time reference for the preceding and succeeding symbols, resulting in built-in symbol synchronization. In other words, DH-PIM creates a symbol to enable built-in symbol synchronization. Thus, like the PPM symbol, the DH-PIM removes the extra time slot after the pulse and increases the average symbol length compared with the PIM, thus increasing data throughput.

Comparisons of modulation techniques wth fixed pulse width are based on various parameters, such as bandwidth occupancy, distortion, SNR, suitability for transmission channels, and error probability. No scheme yields optimal performance and negotiates all signals. For optical transmission, digital pulse time modulation techniques are preferred because of their high peak power and low average power characteristics. They require higher bandwidth than the OOK and provide a higher SNR. The disadvantage of digital pulse time modulation techniques is that they require symbol synchronization and, therefore, more circuitry than other approaches. Tables 1 and 2 summarize the characteristics of M-bit input blocks when they are converted into symbols by the OOK, PPM, DPPM, MPPM, DPIM, and DH-PIM, where R_b is the bit rate and N_0 is the energy of noise [23,26–31,34,35,37,38]. In case of optical communication, the influence of path loss can be ignored, and the received average energy is converted into the maximum energy transmitted, and the received energy per bit E_b, received energy per symbol E_s, and power efficiency η_p are calculated by using this. On the contrary, in case of LIDAR, the maximum energy to be emitted is fixed, and the reflected signal from the object is received. Thus, the influence of path loss must be reflected in the received energy. Therefore, in this paper, energy E_{TX} emitted from LIDAR is reflected off the surface of an object at a distance of R away, and the received energy E_{RX} is calculated by Equation 1. The symbol error rate (SER) is calculated by Equation 2, and the PER by Equation 3 using E_{RX}, which is the received energy according to each modulation technique. Table 3 summarizes the error probability of the digital pulse modulation techniques [23,26,29–31,34,35,37,39–41]. The symbol error rate P_{se} is optimum when the threshold factor k is 0.5.

$$E_{RX} = E_{TX}\frac{\pi\tau_0\tau_a^2 D_R^2\rho_T}{4R^2\theta_R} \tag{1}$$

$$P_{se} = P_0P_{\epsilon 0} + P_1P_{\epsilon 1} = P_0Q\left(k\sqrt{\frac{E_s}{2N_0}}\right) + (1-P_0)\,Q\left((1-k)\sqrt{\frac{E_s}{2N_0}}\right) \tag{2}$$

$$P_{pe} = 1-(1-P_{se})^{\frac{N_{pkt}\bar{L}}{M}} \approx \frac{N_{pkt}\bar{L}}{M}P_{se} \tag{3}$$

Table 1. Comparison of basic characteristics of digital pulse modulation techniques

Modulation	Number of bits (M)	Maximum number of bits (N_p)	Number of possible unique symbols (L)	Maximum number of time slots (L_{max})	Average symbol length ($\bar{L}$)	Slot duration (T_s)
NRZ-OOK	M	M	2^M	M	M	$\frac{1}{R_b}$
PPM	M	1	2^M	L_{PPM}	L_{PPM}	$\frac{1}{R_b}$
DPPM	M	1	2^M	L_{DPPM}	$\frac{L_{DPPM}+1}{2}$	$\frac{1}{R_b}$
MPPM	$\lfloor \log_2 L \rfloor$	w	$\binom{n}{w}$	n	n	$\frac{1}{R_b}$
DPIM	M	1	2^M	L_{DPIM}	$\frac{L_{DPIM}+1}{2}$	$\frac{1}{R_b}$
DH-PIM	M	2	2^M	$2^{M-1}+\alpha$	$\frac{2^{M-1}+2\alpha+1}{2}$	$\frac{1}{R_b}$

Preprints (www.preprints.org) | NOT PEER-REVIEWED | Posted: 5 October 2018 doi:10.20944/preprints201810.0108.v1

Peer-reviewed version available at Sensors 2018, 18, 4201; doi:10.3390/s18124201

Table 2. Comparison of power characteristics of digital pulse modulation techniques

Modulation	Bandwidth requirements (B_{req})	Peak-to-average power ratio (**PAPR**)	Peak current (I_p)	Energy of a pulse (E_p)	Energy of a bit (E_b)
NRZ-OOK	R_b	2	$2\bar{E}_{RX\_OOK}$	$\frac{4\bar{E}^2_{RX\_OOK}}{R_b}$	$\frac{4\bar{E}^2_{RX\_OOK}}{R_b}$
PPM	$\frac{MR_b}{L_{PPM}}$	L_{PPM}	$L_{PPM}\bar{E}_{RX\_PPM}$	$\frac{L^2_{PPM}\bar{E}^2_{RX\_PPM}}{R_b}$	$\frac{L^3_{PPM}\bar{E}^2_{RX\_PPM}}{MR_b}$
DPPM	$\frac{2MR_b}{L_{DPPM}+1}$	2	$2\bar{E}_{RX\_DPPM}$	$\frac{4\bar{E}^2_{RX\_DPPM}}{R_b}$	$\frac{4\bar{E}^3_{RX\_DPPM}}{R_b}$
MPPM	$\frac{MR_b}{n}$	2	$2\bar{E}_{RX\_MPPM}$	$\frac{4\bar{E}^2_{RX\_MPPM}}{R_b}$	$\frac{4\bar{E}^3_{RX\_MPPM}}{R_b}$
DPIM	$\frac{2MR_b}{L_{DPIM}+1}$	2	$2\bar{E}_{RX\_DPIM}$	$\frac{4\bar{E}^2_{RX\_DPIM}}{R_b}$	$\frac{4\bar{E}^3_{RX\_DPIM}}{R_b}$
DH-PIM	$\frac{2MR_b}{2^{M-1}+2\alpha+1}$	2	$2\bar{E}_{RX\_DH-PIM}$	$\frac{4\bar{E}^2_{RX\_DH-PIM}}{R_b}$	$\frac{4\bar{E}^3_{RX\_DH-PIM}}{R_b}$

Table 3. Comparison of error probabilities of digital pulse modulation techniques

Modulation	Probability of "0" (P_0)	Probability of "1" (P_1)	Marginal probability ($P_{\epsilon 0}$)	Optimum symbol error probability (P_{se-opt})
NRZ-OOK	$\frac{1}{2}$	$\frac{1}{2}$	$Q\left(\frac{k\bar{E}_{RX\_OOK}}{\sqrt{N_0R_b}}\right)$	$Q\left(\frac{\bar{E}_{RX\_OOK}}{2\sqrt{N_0R_b}}\right)$
PPM	$\frac{L_{PPM}-1}{L_{PPM}}$	$\frac{1}{L_{PPM}}$	$Q\left(\frac{kL_{PPM}\bar{E}_{RX\_PPM}}{\sqrt{N_0R_b}}\right)$	$Q\left(\frac{L_{PPM}\bar{E}_{RX\_PPM}}{2\sqrt{N_0R_b}}\right)$
DPPM	$\frac{L_{DPPM}-1}{L_{DPPM}+1}$	$\frac{2}{L_{DPPM}+1}$	$Q\left(\frac{k(L_{LPPM}+1)\bar{E}_{RX\_DPPM}}{2\sqrt{N_0R_b}}\right)$	$Q\left(\frac{(L_{DPPM}+1)\bar{E}_{RX\_DPPM}}{4\sqrt{N_0R_b}}\right)$
MPPM	$\frac{n-w}{n}$	$\frac{w}{n}$	$Q\left(\frac{kn\bar{E}_{RX\_MPPM}}{w\sqrt{N_0R_b}}\right)$	$Q\left(\frac{n\bar{E}_{RX\_MPPM}}{4w\sqrt{N_0R_b}}\right)$
DPIM	$\frac{L_{DPIM}-1}{L_{DPIM}+1}$	$\frac{2}{L_{DPIM}+1}$	$Q\left(\frac{k(L_{DPIM}+1)\bar{E}_{RX\_DPIM}}{2\sqrt{N_0R_b}}\right)$	$Q\left(\frac{(L_{DPIM}+1)\bar{E}_{RX\_DPIM}}{4\sqrt{N_0R_b}}\right)$
DH-PIM	$\frac{4\bar{L}_{DH-PIM}-3\alpha}{\bar{L}_{DH-PIM}}$	$\frac{3\alpha}{\bar{L}_{DH-PIM}}$	$Q\left(\frac{2k\left(2^{M-1}+2\alpha+1\right)\bar{E}_{RX\_DH-PIM}}{3\alpha\sqrt{N_0R_b}}\right)$	$Q\left(\frac{\left(2^{M-1}+2\alpha+1\right)\bar{E}_{RX\_DH-PIM}}{3\alpha\sqrt{N_0R_b}}\right)$

2.2. One-dimensional optical spreading codes

Time-division multiple access (TDMA), wavelength-division multiple access (WDMA), and optical code-division multiple access (OCDMA) are techniques of multiple access in optical wireless communications that implement multiplexed transmission and multiple access. Of these, OCDMA supports simultaneous multiple transmissions at the same frequency and the same time slot, and it uses optical spreading codes so that multiple users can be separately identified without interfering with one another. In the simplest type of optical spreading code, one-bit period T_B is divided into M time chips with duration $T_C = \frac{T_B}{M}$, and these M chips are filled with optically spread code. That is, the spreading code sequence is selected to characterize the maximum auto-correlation and minimum cross-correlation to optimize the difference between a correct signal and interference. Primary time spreading codes suitable for OCDMA schemes are OOCs and various PC families. These are very sparse codes, and their code weights are small, thus requiring a long transmission time after spreading.

OOCs are generally expressed as a quadruple $(N, w, \lambda_a, \lambda_c)$, where N is the code length, w is code weight (i.e., the number of ones), λ_a is the upper bound of the autocorrelation value for a non-zero shift, and λ_c is the upper limit of the cross-correlation value [21,42–44]. In the OOC, a particular case where $\lambda_a = \lambda_c = \lambda$ is expressed by the optimal OOC $(N, w, lambda)$. $|C|$ represents the cardinality of the OOC family, i.e., the size of the code set as the number of codewords in the code set. For OOCs to satisfy the condition $\lambda_a = \lambda_c = \lambda = 1$, $|C|$ is upper-bounded by $[C] < \lfloor \frac{N-1}{w(w-1)} \rfloor$, where $\lfloor x \rfloor$ equation denotes the largest integer less than or equal to x. Various algorithms can generate OOC codes that satisfy this condition. By default, the unipolar sequences generated by these algorithms can

Preprints (www.preprints.org) | NOT PEER-REVIEWED | Posted: 5 October 2018 doi:10.20944/preprints201810.0108.v1

Peer-reviewed version available at Sensors 2018, 18, 4201; doi:10.3390/s18124201

all be assumed to be OOC code sets, as long as the code set correlation constraints are met. The code generation of OOC $(N,3,1)$ and OOC $(31,3,1)$ are shown Tables 4 and 5, respectively.

Table 4. OOC $(N,3,1)$ sequence indices for various lengths

N	Sequence index, when $N \leq 49$
7	$\{1,2,4\}$
13	$\{1,2,5\}, \{1,3,8\}$
19	$\{1,2,6\}, \{1,3,9\}, \{1,4,11\}$
25	$\{1,2,7\}, \{1,3,10\}, \{1,4,12\}, \{1,5,14\}$
31	$\{1,2,8\}, \{1,3,12\}, \{1,4,16\}, \{1,5,15\}, \{1,6,14\}$
37	$\{1,2,12\}, \{1,3,10\}, \{1,4,18\}, \{1,5,13\}, \{1,6,19\}, \{1,7,13\}$
43	$\{1,2,20\}, \{1,3,23\}, \{1,4,16\}, \{15,14\}, \{1,6,17\}, \{1,7,15\}, \{1,8,19\}$

Table 5. OOC $(31,3,1)$ sequences

Index	Sequence code
$\{1,2,8\}$	11000 00100 00000 00000 00000 00000 0
$\{1,3,12\}$	10100 00000 01000 00000 00000 00000 0
$\{1,4,16\}$	10010 00000 00000 10000 00000 00000 0
$\{1,5,15\}$	10001 00000 00001 00000 00000 00000 0
$\{1,6,14\}$	10000 10000 00010 00000 00000 00000 0

Compared with OOC, the PC generation process is relatively simple. A code set with a code length of $n = p^2$ and code weight $w = p$ has p unique sequences [21,24,25]. An example of a PC set with $p = 5$ is shown in Table 6. The main disadvantage of PC is that the number of available codes is limited. The code length of PC is only p^2, which may affect the system's performance in terms of bit error rate (BER) and multiple access interference (MAI). Therefore, longer codes that maintain desirable properties are beneficial.

Table 6. Prime code (PC) sequences when $p = 5$

Groups	i					PC sequence	PC sequence code
x	0	1	2	3	4		
0	0	0	0	0	0	S_0	$C_0 = 10000\ 10000\ 10000\ 10000\ 10000$
1	0	1	2	3	4	S_1	$C_1 = 10000\ 01000\ 00100\ 00010\ 00001$
2	0	2	4	1	3	S_2	$C_2 = 10000\ 00100\ 00001\ 01000\ 00010$
3	0	3	1	4	2	S_3	$C_3 = 10000\ 00010\ 01000\ 00001\ 00100$
4	0	4	3	2	1	S_4	$C_4 = 10000\ 00001\ 00010\ 10000\ 01000$

As the cardinality of the PC corresponds to the number of users, M, it is equal to w, of the PC, and w is equal to the prime number p; thus, p must be increased. To increase the number of users on the network, weight w must be greater. A modified prime code (MPC) has been proposed to overcome the drawbacks of the PC [21,24,25,45]. This optical sequence eliminates some redundant pulses from the original PC with a pulse, assuming a BER requirement such as 10^{-9} and a certain number of users. The weight of the MPC is smaller than that of the PC, but the code can support the p group containing p sequences and p^2 subscribers having the same code sequence length as p^2. The configuration of MPC is as follows: Generate the PC with p codewords. Any $p - w$ pulse is removed from this PC, and the remaining pulses form a new code with a constant weight w. The length, the weight, and the cardinality of MPC are n, $w < p$, and $|C| = p$, respectively. An example of an MPC set with $p = 5$ and $w = 4$ is shown in Table 7.

Peer-reviewed version available at Sensors 2018, 18, 4201; doi:10.3390/s18124201

Table 7. Modified prime code (MPC) sequences S_i' constructed for $p = 5$ and $w = 4$

Groups	i				MPC sequence	MPC sequence code
x	a_0	a_1	a_2	a_3		
0	0	0	0	0	S_0'	$C_0' =$ 10000 10000 10000 10000 00000
1	0	1	2	3	S_1'	$C_1' =$ 10000 01000 00100 00010 00000
2	0	2	4	1	S_2'	$C_2' =$ 10000 00100 00001 01000 00000
3	0	3	1	4	S_3'	$C_3' =$ 10000 00010 01000 00001 00000
4	0	4	3	2	S_4'	$C_4' =$ 10000 00001 00010 10000 00000

Table 8 summarizes the characteristics of OOC, PC, and MPC including length, weight, peak auto-correlation and cross-correlation, cardinality, and error probability [21,24,25,42–52].

Table 8. Performance comparison of optical spreading codes

characteristics	OOC (N, w, λ)	PC	MPC
Length	N	p^2	p^2
Weight	w	p	w
Peak auto-correlation	1	$p-1$	0
Peak cross-correlation	1	2	0
Cardinality	$\lfloor \frac{N-1}{w(w-1)} \rfloor$	p	p
Error probability	$\frac{1}{2}\sum_{i=0}^{w}(-1)^i\binom{w}{i}\left(1-\frac{iw}{2n}\right)^{M-1}$	$\frac{1}{2}\sum_{i=0}^{p}(-1)^i\binom{p}{i}\left(1-\frac{i}{2p}\right)^{M-1}$	$\frac{1}{2}\sum_{i=0}^{\frac{w}{2}}(-1)^i\binom{\frac{w}{2}}{i}\left(1-\frac{iw^2}{2p^2}\right)^{M-1}$

3. Performance evaluation of combinations of modulation and spreading code techniques

3.1. Combinations of modulation and spreading code techniques

To evaluate the performance of the modulation and spreading code schemes used in the prototype LIDAR system, several operating conditions have been specified according to the characteristics of the prototype LIDAR system [18,19]. At each pixel, the prototype LIDAR system generates pixel information to identify the measuring point and emission time. Pixel information is represented by a nine-bit stream consisting of a leading "1," a five-bit column identification number (CID), and a three-bit cyclic redundancy check (CRC) checksum. The CID represents the locations of corresponding pixels for each measurement angle and identifies each of the 30 columns from a 30×30 range image.

- A nine-bit block is used to identify each measurement point, and the first bit is always "1"
- Up to five measurement points can be measured simultaneously
- Pulse width is fixed at 5 ns and pulse transmission is completed within 67 µs
- The maximum output of the laser pulse is eye-safety class 1 compliant
- The maximum desired distance: 150 m
- Range gate: 1 µs
- Probability of false alarm: 0.5
- False alarm rate: 500.000/s
- TNR: 9.8 dB

Table 9 shows the eight symbols that can be expressed in three-bit blocks according to the OOK, PPM, DPPM, MPPM, DPIM, and DH-PIM. The OOK, PPM, and MPPM have a fixed number of slots regardless of symbol values, and the DPPM, DPIM, and DH-PIM vary in the number of slots according to symbol values. The OOK, PPM, and MPPM can know the transmitted symbol by detecting the start and end of the pulse. As all three know the end if they detect the start, they should add a leading "1" to indicate the start of the transmission before the first symbol. As the DPPM ends with "1", the symbol

can be known by the number of "0s" transmitted before "1" is reached. The DPIM and DH-PIM can identify symbols with a number of "0s" after a "1" and cannot know the symbols because the number of "0s" in the last symbol is unknown. In this case, we should mark the end of the transmission by appending a trailing "1" to the end of the last symbol. We use zero GSs for the modulation techniques because optical spreading codes are very sparse codes, and two or more successive "0s" precede a very sparse "1."

Table 9. Three-bit block representation according to modulation technique

Source symbol	OOK	8-PPM	8-DPPM	2-5MPPM	8-DPIM	8-DH-PIM$_2$
0	000	10000000	1	10001	1	100
1	001	01000000	01	01100	10	1000
2	010	00100000	001	01001	100	10000
3	011	00010000	0001	10010	1000	100000
4	100	00001000	00001	11000	10000	110000
5	101	00000100	000001	00101	100000	11000
6	110	00000010	0000001	00011	1000000	1100
7	111	00000001	00000001	10100	10000000	110

The possible modulation schemes according to the size of the bit input block are shown in Table 10. As slot size increases, the number of slots required for modulation increase linearly in the OOK, but those in the PPM, DPPM, DPIM, and DH-PIM increase exponentially, and that of the MPPM increases exponentially but relatively mildly.

Table 10. Possible modulation schemes according to the size of the bit input block

Block size	OOK	8-PPM	8-DPPM	2-5MPPM	8-DPIM	8-DH-PIM$_2$
1-bit	1, 1	1, 2	1, 2	2, 3	1, 2	2, 3
2-bit	2, 2	1, 4	1, 4	2, 4	1, 4	2, 4
3-bit	3, 3	1, 8	1, 8	2, 5	1, 8	2, 6
4-bit	4, 4	1, 16	1, 16	2, 6	1, 16	2, 10
5-bit	5, 5	1, 32	1, 32	2, 9	1, 32	2, 18
6-bit	6, 6	1, 64	1, 64	2, 12	1, 64	2, 34
7-bit	7, 7	1, 128	1, 128	2, 17	1, 128	2, 66
8-bit	8, 8	1, 256	1, 256	2, 24	1, 256	2, 129
9-bit	9, 9	1, 512	1, 512	2, 33	1, 512	2, 258

If the bit input block is partitioned into several block sizes according to Table 8, the number of slots according to each modulation scheme is as shown in Table 11. In the block partitioning column, the OOK, PPM, DPPM, and MPPM use a leading "1" to indicate the start of transmission, and the DPIM and DH-PIM use a trailing "1" to indicate its end. Splitting the bit input block into several smaller partitions requires fewer slots to be transferred than using a single large partition. However, as the number of "1s" for transmitting pulses is determined according to the number of partitions, the number of pulses to be transmitted increases when a plurality of small partitions is used and decreases when a large partition is used. The prototype LIDAR system is a non-directional non-line of sight (NLOS) optical wireless communication system that uses Lambertian diffusion. Eye safety is a critical issue in optical wireless systems because optical signals can penetrate the human cornea and potentially cause thermal damage to the retina. Optical transmitters must comply with the class 1 of the International Electrotechnical Commission (IEC) standard. The MPE is the highest power or energy density of a light source considered safe, i.e., less likely to cause damage.

Preprints (www.preprints.org) | NOT PEER-REVIEWED | Posted: 5 October 2018 doi:10.20944/preprints201810.0108.v1

Peer-reviewed version available at Sensors 2018, 18, 4201; doi:10.3390/s18124201

Table 11. Possible block partitioning according to modulation techniques. A bold "**1**" shows a leading "1" or a trailing "1."

Block paritioning	OOK	PPM	DPPM	MPPM	DPIM	DH-PIM$_2$
1 : 2 : 2 : 2 : 2	9, 9	5, 17	5, 17	9, 17		
2 : 2 : 2 : 2 : **1**					5, 17	9, 17
1 : 2 : 3 : 3	9, 9	4, 21	4, 21	7, 15		
2 : 3 : 3 : **1**					4, 21	7, 17
1 : 4 : 4	9, 9	3, 33	3, 33	5, 13		
4 : 4 : **1**					3, 33	5, 21
1 : 5 : 3	9, 9	3, 41	3, 41	5, 15		
5 : 3 : **1**					3, 41	5, 25
1 : 8	9, 9	2, 257	2, 257	3, 25		
8 : **1**					2, 257	3, 131

The combination of modulation and spreading code techniques is determined to satisfy all operating conditions of the prototype LIDAR. The following operating characteristics are determined according to the combinations:

- Symbol stream
- Block size and partitioning
- Pulse peak power
- Number of time slots
- Number of pulses
- leading "1" or trailing "1"

If the bit input block is divided into partitions of various sizes and the optical spreading code with a cardinality of five is applied, the transmission characteristics are as shown in Tables 12 and 13. The number of time slots needed for transmission is the greatest, and each pair relates the number of slots, the number of pulses, and the maximum pulse output. The transmission power of the pulse is inversely proportion to the number of transmitted pulses.

Table 12. Number of pulses and time slots as combination of modulation and spreading code

Spreading codes	OOK	PPM	DPPM	MPPM	DPIM	DH-PIM$_2$
Block partitioning	1 : 2 : 2 : 2 : 2	1 : 2 : 2 : 2 : 2	1 : 2 : 2 : 2 : 2	1 : 2 : 2 : 2 : 2	2 : 2 : 2 : 2 : 1	2 : 2 : 2 : 2 : 1
OOC $(31, 3, 1)$	279, 27	527, 15	527, 15	527, 27	527, 15	527, 27
PC $p = 5$	225, 45	425, 25	425, 25	425, 45	425, 25	425, 45
MPC $p = 5,\ w = 4$	225, 36	425, 20	425, 20	425, 36	425, 20	425, 36
Block partitioning	1 : 2 : 3 : 3	1 : 2 : 3 : 3	1 : 2 : 3 : 3	1 : 2 : 3 : 3	2 : 3 : 3 : 1	2 : 3 : 3 : 1
OOC $(31, 3, 1)$	279, 27	651, 12	651, 12	465, 21	651, 12	527, 21
PC $p = 5$	225, 45	525, 20	525, 20	375, 35	525, 20	425, 35
MPC $p = 5,\ w = 4$	225, 36	525, 16	525, 16	375, 28	525, 16	425, 28
Block partitioning	1 : 4 : 4	1 : 4 : 4	1 : 4 : 4	1 : 4 : 4	4 : 4 : 1	4 : 4 : 1
OOC $(31, 3, 1)$	279, 27	1023, 9	1023, 9	403, 15	1023, 9	651, 15
PC $p = 5$	225, 45	825, 15	825, 15	325, 25	825, 15	525, 25
MPC $p = 5,\ w = 4$	225, 36	825, 12	825, 12	325, 20	825, 12	525, 20
Block partitioning	1 : 2 : 2 : 2 : 2	1 : 2 : 2 : 2 : 2	1 : 2 : 2 : 2 : 2	1 : 2 : 2 : 2 : 2	2 : 2 : 2 : 2 : 1	2 : 2 : 2 : 2 : 1
OOC $(31, 3, 1)$	279, 27	1271, 9	1271, 9	465, 15	1271, 9	775, 15
PC $p = 5$	225, 45	1025, 15	1025, 15	375, 25	1025, 15	625, 25
MPC $p = 5,\ w = 4$	225, 36	1025, 12	1025, 12	375, 20	1025, 12	625, 20
Block partitioning	1 : 8	1 : 8	1 : 8	1 : 8	8 : 1	8 : 1
OOC $(31, 3, 1)$	279, 27	7967, 6	7967, 6	775, 15	7967, 6	4061, 9
PC $p = 5$	225, 45	6425, 10	6425, 10	625, 25	6425, 10	3275, 15
MPC $p = 5,\ w = 4$	225, 36	6425, 8	6425, 8	625, 20	6425, 8	3275, 12

Preprints (www.preprints.org) | NOT PEER-REVIEWED | Posted: 5 October 2018 doi:10.20944/preprints201810.0108.v1

Peer-reviewed version available at Sensors 2018, 18, 4201; doi:10.3390/s18124201

Table 13. Number of pulses and time slots as combination of modulation and spreading code

Spreading codes	OOK	PPM	DPPM	MPPM	DPIM	DH-PIM$_2$
Block partitioning	1 : 2 : 2 : 2 : 2	1 : 2 : 2 : 2 : 2	1 : 2 : 2 : 2 : 2	1 : 2 : 2 : 2 : 2	2 : 2 : 2 : 2 : 1	2 : 2 : 2 : 2 : 1
OOC $(31, 3, 1)$	8.9143 nJ	10.3254 nJ	10.3254 nJ	8.9143 nJ	10.3254 nJ	8.9143 nJ
PC $p = 5$	7.8456 nJ	9.0895 nJ	9.0895 nJ	7.8456 nJ	9.0895 nJ	7.8456 nJ
MPC $p = 5$, $w = 4$	8.2957 nJ	9.6088 nJ	9.6088 nJ	8.2957 nJ	9.6088 nJ	8.2957 nJ
Block partitioning	1 : 2 : 3 : 3	1 : 2 : 3 : 3	1 : 2 : 3 : 3	1 : 2 : 3 : 3	2 : 3 : 3 : 1	2 : 3 : 3 : 1
OOC $(31, 3, 1)$	8.9143 nJ	10.9178 nJ	10.9178 nJ	9.4923 nJ	10.9178 nJ	9.4923 nJ
PC $p = 5$	7.8456 nJ	9.6088 nJ	9.6088 nJ	8.4543 nJ	9.6088 nJ	8.4543 nJ
MPC $p = 5$, $w = 4$	8.2957 nJ	10.1601 nJ	10.1601 nJ	8.8336 nJ	10.1601 nJ	8.8336 nJ
Block partitioning	1 : 4 : 4	1 : 4 : 4	1 : 4 : 4	1 : 4 : 4	4 : 4 : 1	4 : 4 : 1
OOC $(31, 3, 1)$	8.9143 nJ	11.7319 nJ	11.7319 nJ	10.3254 nJ	11.7319 nJ	10.3254 nJ
PC $p = 5$	7.8456 nJ	10.3254 nJ	10.3254 nJ	9.0895 nJ	10.3254 nJ	9.0895 nJ
MPC $p = 5$, $w = 4$	8.2957 nJ	10.9178 nJ	10.9178 nJ	9.6088 nJ	10.9178 nJ	9.6088 nJ
Block partitioning	1 : 2 : 2 : 2 : 2	1 : 2 : 2 : 2 : 2	1 : 2 : 2 : 2 : 2	1 : 2 : 2 : 2 : 2	2 : 2 : 2 : 2 : 1	2 : 2 : 2 : 2 : 1
OOC $(31, 3, 1)$	8.9143 nJ	11.7319 nJ	11.7319 nJ	10.3254 nJ	11.7319 nJ	10.3254 nJ
PC $p = 5$	7.8456 nJ	10.3254 nJ	10.3254 nJ	9.0895 nJ	10.3254 nJ	9.0895 nJ
MPC $p = 5$, $w = 4$	8.2957 nJ	10.9178 nJ	10.9178 nJ	9.6088 nJ	10.9178 nJ	9.6088 nJ
Block partitioning	1 : 8	1 : 8	1 : 8	1 : 8	8 : 1	8 : 1
OOC $(31, 3, 1)$	8.9143 nJ	12.9835 nJ	12.9835 nJ	10.3254 nJ	12.9835 nJ	11.7319 nJ
PC $p = 5$	7.8456 nJ	11.4269 nJ	11.4269 nJ	9.0895 nJ	11.4269 nJ	10.3254 nJ
MPC $p = 5$, $w = 4$	8.2957 nJ	12.0825 nJ	12.0825 nJ	9.6088 nJ	12.0825 nJ	10.9178 nJ

3.2. Performance evaulation of combined techniques

The experimental environment was the same as that for the prototype LIDAR system, and a modulation technique and a spreading code technique was used. Experiments were conducted using various parameters on a table with a 2 × 2m white paper wall as shown in Figure 3. We evaluated the performance of the following elements based on combinations of various modulation and spreading code techniques as well as the operating characteristics of the prototype LIDAR system [18,19].

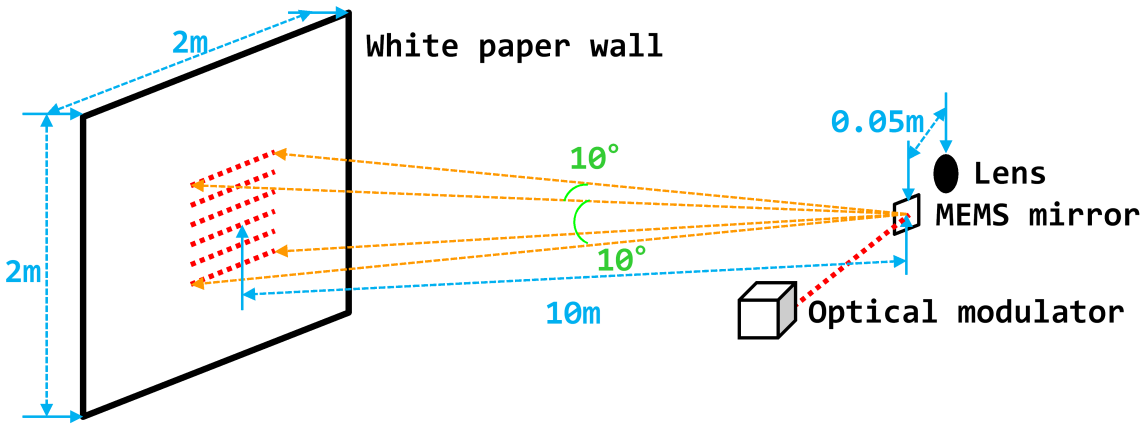

Figure 3. Experimental conditions and optical structure of the prototype LIDAR systems

The prototype LIDAR system uses optical communication technology in LIDAR and, therefore, evaluates its performance concerning both the characteristics of LIDAR and those of wireless communication. As LIDAR is a distance-measuring device, the maximum distance obtained is shown in Table 14, and the accuracy and precision are shown in Tables 15 and 16, respectively. The maximum distance was determined by the TNR [3,5,10,11,19,53]. Using the result of the measured power and the relationship between the received power measured distance, and target surface reflectivity illustrated in Equation 1, we estimated the received power based on the distance. Accuracy and precision were determined using the American Society for Photogrammetry and Remote Sensing (ASPRS)'s positional

standards for digital elevation data [54,55]. The maximum measurement distance of the pulse was proportional to the number of transmitted pulses, as were accuracy and precision .

Table 14. Maximum distance as a combination of modulation and spreading code

Spreading codes	OOK	PPM	DPPM	MPPM	DPIM	DH-PIM$_2$
Block partitioning	1 : 2 : 2 : 2 : 2	1 : 2 : 2 : 2 : 2	1 : 2 : 2 : 2 : 2	1 : 2 : 2 : 2 : 2	2 : 2 : 2 : 2 : 1	2 : 2 : 2 : 2 : 1
OOC $(31,3,1)$	95 m	102 m	102 m	95 m	102 m	95 m
PC $p = 5$	89 m	96 m	96 m	89 m	96 m	89 m
MPC $p = 5$, $w = 4$	91 m	98 m	98 m	91 m	98 m	91 m
Block partitioning	1 : 2 : 3 : 3	1 : 2 : 3 : 3	1 : 2 : 3 : 3	1 : 2 : 3 : 3	2 : 3 : 3 : 1	2 : 3 : 3 : 1
OOC $(31,3,1)$	95 m	105 m	105 m	98 m	105 m	98 m
PC $p = 5$	89 m	98 m	98 m	92 m	98 m	92 m
MPC $p = 5$, $w = 4$	91 m	101 m	101 m	94 m	101 m	94 m
Block partitioning	1 : 4 : 4	1 : 4 : 4	1 : 4 : 4	1 : 4 : 4	4 : 4 : 1	4 : 4 : 1
OOC $(31,3,1)$	95 m	109 m	109 m	102 m	109 m	102 m
PC $p = 5$	89 m	102 m	102 m	96 m	102 m	96 m
MPC $p = 5$, $w = 4$	91 m	105 m	105 m	98 m	105 m	98 m
Block partitioning	1 : 2 : 2 : 2 : 2	1 : 2 : 2 : 2 : 2	1 : 2 : 2 : 2 : 2	1 : 2 : 2 : 2 : 2	2 : 2 : 2 : 2 : 1	2 : 2 : 2 : 2 : 1
OOC $(31,3,1)$	95 m	109 m	109 m	102 m	109 m	102 m
PC $p = 5$	89 m	102 m	102 m	96 m	102 m	96 m
MPC $p = 5$, $w = 4$	91 m	105 m	105 m	98 m	105 m	98 m
Block partitioning	1 : 8	1 : 8	1 : 8	1 : 8	8 : 1	8 : 1
OOC $(31,3,1)$	95 m	114 m	114 m	102 m	114 m	109 m
PC $p = 5$	89 m	107 m	107 m	96 m	107 m	102 m
MPC $p = 5$, $w = 4$	91 m	110 m	110 m	98 m	110 m	105 m

Table 15. Accuracy as a combination of modulation and spreading code

Spreading codes	OOK	PPM	DPPM	MPPM	DPIM	DH-PIM$_2$
Block partitioning	1 : 2 : 2 : 2 : 2	1 : 2 : 2 : 2 : 2	1 : 2 : 2 : 2 : 2	1 : 2 : 2 : 2 : 2	2 : 2 : 2 : 2 : 1	2 : 2 : 2 : 2 : 1
OOC $(31,3,1)$	29.19 mm	30.16 mm	30.41 mm	29.19 mm	30.16 mm	29.51 mm
PC $p = 5$	29.05 mm	29.72 mm	29.25 mm	29.05 mm	29.47 mm	29.05 mm
MPC $p = 5$, $w = 4$	29.12 mm	29.99 mm	29.33 mm	29.21 mm	29.54 mm	29.64 mm
Block partitioning	1 : 2 : 3 : 3	1 : 2 : 3 : 3	1 : 2 : 3 : 3	1 : 2 : 3 : 3	2 : 3 : 3 : 1	2 : 3 : 3 : 1
OOC $(31,3,1)$	29.57 mm	30.60 mm	31.06 mm	29.61 mm	30.43 mm	29.93 mm
PC $p = 5$	28.86 mm	29.59 mm	30.11 mm	29.28 mm	29.46 mm	29.31 mm
MPC $p = 5$, $w = 4$	29.45 mm	29.89 mm	30.06 mm	29.49 mm	30.03 mm	29.96 mm
Block partitioning	1 : 4 : 4	1 : 4 : 4	1 : 4 : 4	1 : 4 : 4	4 : 4 : 1	4 : 4 : 1
OOC $(31,3,1)$	29.43 mm	30.67 mm	32.36 mm	29.47 mm	30.62 mm	30.18 mm
PC $p = 5$	29.28 mm	29.99 mm	30.29 mm	29.34 mm	30.73 mm	29.33 mm
MPC $p = 5$, $w = 4$	29.10 mm	30.36 mm	30.17 mm	29.26 mm	30.54 mm	29.48 mm
Block partitioning	1 : 2 : 2 : 2 : 2	1 : 2 : 2 : 2 : 2	1 : 2 : 2 : 2 : 2	1 : 2 : 2 : 2 : 2	2 : 2 : 2 : 2 : 1	2 : 2 : 2 : 2 : 1
OOC $(31,3,1)$	29.98 mm	31.14 mm	31.37 mm	30.14 mm	31.47 mm	30.64 mm
PC $p = 5$	29.57 mm	30.44 mm	30.12 mm	29.23 mm	30.47 mm	30.27 mm
MPC $p = 5$, $w = 4$	29.66 mm	30.56 mm	30.91 mm	29.58 mm	30.91 mm	29.74 mm
Block partitioning	1 : 8	1 : 8	1 : 8	1 : 8	8 : 1	8 : 1
OOC $(31,3,1)$	29.92 mm	32.88 mm	32.31 mm	30.34 mm	32.82 mm	31.95 mm
PC $p = 5$	29.11 mm	30.56 mm	31.13 mm	29.70 mm	30.93 mm	30.30 mm
MPC $p = 5$, $w = 4$	29.34 mm	31.54 mm	31.71 mm	29.55 mm	31.86 mm	31.05 mm

Preprints (www.preprints.org) | NOT PEER-REVIEWED | Posted: 5 October 2018 doi:10.20944/preprints201810.0108.v1

Peer-reviewed version available at Sensors 2018, 18, 4201; doi:10.3390/s18124201

Table 16. Precision as a combination of modulation and spreading code

Spreading codes	OOK	PPM	DPPM	MPPM	DPIM	DH-PIM$_2$
Block partitioning	1 : 2 : 2 : 2 : 2	1 : 2 : 2 : 2 : 2	1 : 2 : 2 : 2 : 2	1 : 2 : 2 : 2 : 2	2 : 2 : 2 : 2 : 1	2 : 2 : 2 : 2 : 1
OOC $(31, 3, 1)$	3.74 mm	4.86 mm	4.85 mm	3.74 mm	4.91 mm	3.60 mm
PC $p = 5$	2.89 mm	3.93 mm	3.69 mm	2.89 mm	3.78 mm	2.87 mm
MPC $p = 5,\ w = 4$	3.12 mm	4.14 mm	4.03 mm	3.12 mm	4.41 mm	3.24 mm
Block partitioning	1 : 2 : 3 : 3	1 : 2 : 3 : 3	1 : 2 : 3 : 3	1 : 2 : 3 : 3	2 : 3 : 3 : 1	2 : 3 : 3 : 1
OOC $(31, 3, 1)$	3.69 mm	5.52 mm	5.52 mm	4.06 mm	5.58 mm	4.29 mm
PC $p = 5$	2.83 mm	4.21 mm	4.30 mm	3.19 mm	4.27 mm	3.11 mm
MPC $p = 5,\ w = 4$	3.14 mm	4.85 mm	4.87 mm	3.42 mm	4.78 mm	3.69 mm
Block partitioning	1 : 4 : 4	1 : 4 : 4	1 : 4 : 4	1 : 4 : 4	4 : 4 : 1	4 : 4 : 1
OOC $(31, 3, 1)$	3.68 mm	6.24 mm	6.55 mm	5.05 mm	6.40 mm	5.03 mm
PC $p = 5$	2.85 mm	5.03 mm	5.03 mm	3.76 mm	4.88 mm	3.80 mm
MPC $p = 5,\ w = 4$	3.25 mm	5.35 mm	5.49 mm	4.31 mm	5.62 mm	4.17 mm
Block partitioning	1 : 2 : 2 : 2 : 2	1 : 2 : 2 : 2 : 2	1 : 2 : 2 : 2 : 2	1 : 2 : 2 : 2 : 2	2 : 2 : 2 : 2 : 1	2 : 2 : 2 : 2 : 1
OOC $(31, 3, 1)$	3.68 mm	6.22 mm	6.39 mm	4.99 mm	6.13 mm	4.96 mm
PC $p = 5$	2.81 mm	5.20 mm	4.97 mm	3.85 mm	5.25 mm	3.96 mm
MPC $p = 5,\ w = 4$	3.33 mm	5.52 mm	5.53 mm	4.24 mm	5.66 mm	4.32 mm
Block partitioning	1 : 8	1 : 8	1 : 8	1 : 8	8 : 1	8 : 1
OOC $(31, 3, 1)$	3.83 mm	7.82 mm	7.68 mm	4.92 mm	7.81 mm	6.51 mm
PC $p = 5$	2.81 mm	6.05 mm	5.95 mm	3.86 mm	5.82 mm	5.04 mm
MPC $p = 5,\ w = 4$	3.23 mm	6.91 mm	6.77 mm	4.09 mm	6.97 mm	5.61 mm

OOK allocates one time slot per bit, so the number of time slots is constant regardless of the partitioning of the block. PPM, DPPM, and DPIM are different from each other in their numbers of "1s" and their average symbol sizes, but their number of time slots is the same according to the maximum symbol size, indicating whether a transmission is possible within a given time. These three modulation methods are identical regarding the parameters required to measure the performance of the LIDAR system, even though the symbol representation is different. The DH-PIM has the advantage that the average and maximum symbol sizes are both smaller than those of PPM, DPPM, and DPIM. However, it has a disadvantage that the number of "1s" required for representing a block is large. If the number of slots corresponding to "1" is large, the pulse peak power is small, and the maximum measurement distance is shortened, but the accuracy and precision are improved. Unlike other modulation methods in which the number of "1s" is fixed, DH-PIM changes the number of "1s" according to the symbol. If the pulse peak power can be changed dynamically according to the number of "1s", a longer pulse distance can be measured using the pulse peak power when the number of "1s" is small. MPPM has the advantage that the average and maximum symbol sizes are the smallest modulation schemes. However, as in the case of DH-PIM, the number of "1s" needed to represent a symbol is increased, so the pulse peak power is reduced. As a result, the maximum measurement distance is shortened, but accuracy and precision are improved. Compared to other modulation methods, MPPM exhibits the best balance of measurement distance, precision, and accuracy.

The combination of using OOK as the modulation technique and PC or MPC as the spreading code technique has the smallest number of time slots. In this case, the number of time slots is always 225, regardless of the size of the block partition. When the block is divided into 8 bits, the PPM is used as the modulation method, and the OOC is used as the spreading code technique, the highest number of time slots is required. In this case, a total of 7969 time slots are required, and since one time slot is allocated 5 ns, 39.835 µs are required to complete the transmission. In this worst case, the transmission is completed within the allowed 67 µs of the prototype LIDAR system, so a combination of all possible modulation and spreading code techniques is possible. When the number of pulses is the smallest, the maximum measurement distance difference is 25 m, the accuracy difference is 3.2 mm, and the precision difference is 4.87 mm. In evaluating the performance of the LIDAR system, the maximum measurement distance is given priority over accuracy and precision, and the difference between the accuracy and the precision according to the modulation technique is negligible. Therefore,

Preprints (www.preprints.org) | NOT PEER-REVIEWED | Posted: 5 October 2018 doi:10.20944/preprints201810.0108.v1

Peer-reviewed version available at Sensors 2018, 18, 4201; doi:10.3390/s18124201

in the LIDAR system, it is best to use the combination with the least number of pulses satisfying the maximum allowable transmission time. Of the combinations we evaluated, the combination of using PPM, DPPM, or DPIM as the modulation technique and using OOC as the spreading code technique can measure the farthest distance. Figure 4 shows the overall relationship between the measured results and combinations of modulation and spreading codes.

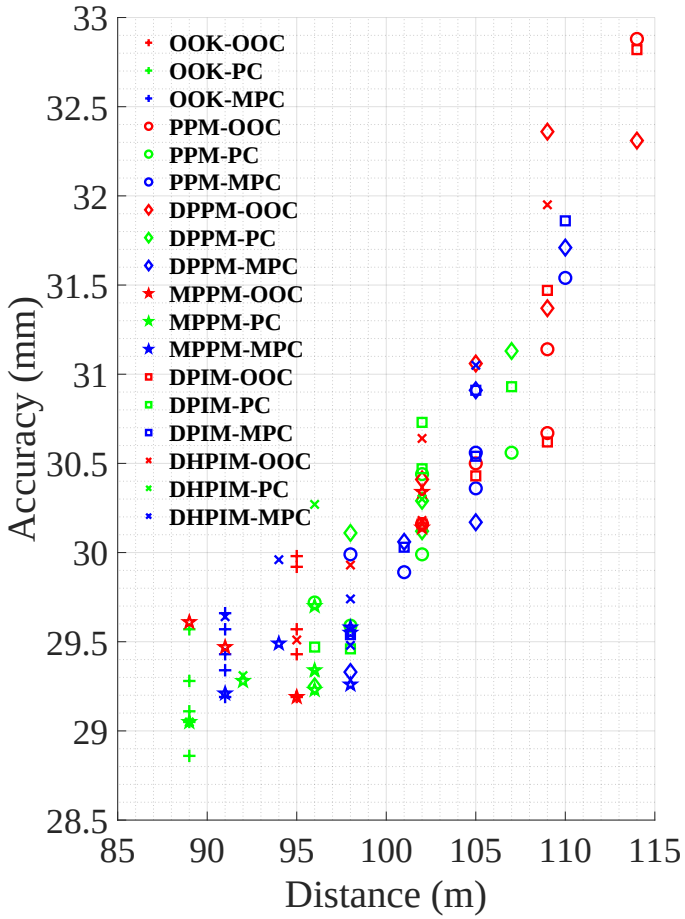

Figure 4. Relationship between the maximum distance and accuracy

As the prototype LIDAR system applies the communication scheme, the PER according to the combination of the modulation scheme and the spreading scheme used for transmission is shown in Table 17. If an error occurred when a packet was received at the LIDAR, the result of distance measurement for the relevant measurement point was ignored. The combination of all the modulation and spreading codes we evaluated showed such a low PER. As long as the number of points to be measured does not exceed the cardinality of the spreading code, the current combinations can be used reliably.

Table 17. Packet error rate (PER) as a combination of modulation and spreading code

Spreading codes	OOK	PPM	DPPM	MPPM	DPIM	DH-PIM$_2$
Block partitioning	1 : 2 : 2 : 2 : 2	1 : 2 : 2 : 2 : 2	1 : 2 : 2 : 2 : 2	1 : 2 : 2 : 2 : 2	2 : 2 : 2 : 2 : 1	2 : 2 : 2 : 2 : 1
OOC $(31, 3, 1)$	0.006 19	0.000 08	0.000 08	0.000 68	0.000 08	0.000 68
PC $p = 5$	0.025 04	0.000 53	0.000 53	0.002 80	0.000 53	0.002 80
MPC $p = 5$, $w = 4$	0.014 15	0.000 26	0.000 26	0.001 58	0.000 26	0.001 58
Block partitioning	1 : 2 : 3 : 3	1 : 2 : 3 : 3	1 : 2 : 3 : 3	1 : 2 : 3 : 3	2 : 3 : 3 : 1	2 : 3 : 3 : 1
OOC $(31, 3, 1)$	0.006 19	0.000 03	0.000 03	0.000 30	0.000 03	0.000 30
PC $p = 5$	0.025 04	0.000 26	0.000 26	0.001 45	0.000 26	0.001 45
MPC $p = 5$, $w = 4$	0.014 15	0.000 11	0.000 11	0.000 75	0.000 11	0.000 75
Block partitioning	1 : 4 : 4	1 : 4 : 4	1 : 4 : 4	1 : 4 : 4	4 : 4 : 1	4 : 4 : 1
OOC $(31, 3, 1)$	0.006 19	0.000 01	0.000 01	0.000 08	0.000 01	0.000 08
PC $p = 5$	0.025 04	0.000 08	0.000 08	0.000 53	0.000 08	0.000 53
MPC $p = 5$, $w = 4$	0.014 15	0.000 03	0.000 03	0.000 26	0.000 03	0.000 26
Block partitioning	1 : 2 : 2 : 2 : 2	1 : 2 : 2 : 2 : 2	1 : 2 : 2 : 2 : 2	1 : 2 : 2 : 2 : 2	2 : 2 : 2 : 2 : 1	2 : 2 : 2 : 2 : 1
OOC $(31, 3, 1)$	0.006 19	0.000 01	0.000 01	0.000 08	0.000 01	0.000 08
PC $p = 5$	0.025 04	0.000 08	0.000 08	0.000 53	0.000 08	0.000 53
MPC $p = 5$, $w = 4$	0.014 15	0.000 03	0.000 03	0.000 26	0.000 03	0.000 26
Block partitioning	1 : 8	1 : 8	1 : 8	1 : 8	8 : 1	8 : 1
OOC $(31, 3, 1)$	0.006 19	0.000 00	0.000 00	0.000 08	0.000 00	0.000 01
PC $p = 5$	0.025 04	0.000 01	0.000 01	0.000 53	0.000 01	0.000 08
MPC $p = 5$, $w = 4$	0.014 15	0.000 00	0.000 00	0.000 26	0.000 00	0.000 03

4. Conclusions

In case of LIDAR with pulse coding, the pulse peak power and the maximum measurable distance both increase inversely proportionally to the number of transmitted pulses to comply with eye safety standards, and accuracy and precision increase in proportion to the number of pulses. Therefore, dividing the bit input block into several smaller partitions reduces transmission time and the maximum measurement distance and improves accuracy and precision. Conversely, dividing the bit input block into large partitions increases the transfer time and maximum measurement distance but reduces precision and accuracy. It is thus useful to select a modulation and a spread coding scheme according to the use and conditions of operation of LIDAR. If we need to measure distances even if accuracy and precision are low, we should use a combination of the smallest number of pulses and the smallest number of slots to increase the number of measurement points per second. In case of prioritizing accuracy and precision, the combination with the largest number of pulses is preferable.

Author Contributions: Gunzung Kim conducted experiments and wrote the manuscript under the supervision of Yongwan Park.

Funding: This research was funded by the Information Technology Research Center (ITRC) support program (IITP-2018-2016-0-00313) and the Basic Science Research Program (2017R1E1A1A01074345).

Conflicts of Interest: The authors declare no conflict of interest.

References

1. Amann, M.C.; Bosch, T.; Lescure, M.; Myllyla, R.; Rioux, M. Laser Ranging: A Critical Review of Usual Techniques for Distance Measurement. *Opt. Eng.* **2001**, *40*, 10–19.
2. Hancock, J. Laser Intensity–Based Obstacle Detection and Tracking. PhD thesis, Robotics Institute, Carnegie Mellon University, Pittsburgh, PA, USA, 1999.
3. Richmond, R.D.; Cain, S.C. *Direct–Detection LADAR Systems*; Vol. TT85, *Tutorial texts in optical engineering*, International Society for Optics and Photonics: Bellingham, Washington, USA, 2010.
4. McManamon, P.F. Review of LADAR: A Historic, Yet Emerging, Sensor Technology with Rich Phenomenology. *Opt. Eng.* **2012**, *51*, 060901.
5. McManamon, P.F. *Field Guide to Lidar*; Vol. FG36, *Field Guide*, International Society for Optics and Photonics: Bellingham, Washington, USA, 2015.

6. Süss, A.; Rochus, V.; Rosmeulen, M.; Rottenberg, X. Benchmarking Time–of–Flight Based Depth Measurement Techniques. Proc. SPIE **9751**. International Society for Optics and Photonics, 2016, p. 975118.
7. SICK AG. *Operating Instructions for Laser Measurement Sensors of the LMS5xx Product Family*. Waldkirch, Germany, 2015.
8. Velodyne. *HDL–64E S3 Users's Manual and Programming Guide*. San Jose, CA, USA, 2013.
9. Behroozpour, B.; Sandborn, P.A.; Wu, M.C.; Boser, B.E. LIDAR System Architectures and Circuits. *IEEE Communications Magazine* **2017**, *55*, 135–142.
10. RCA. *Electro-Optics Handbook*; RCA: New York, NY, USA, 1974.
11. Burns, H.N.; Christodoulou, C.G.; Boreman, G.D. System design of a pulsed laser rangefinder. *Opt. Eng.* **1991**, *30*, 323–329.
12. Ogilvy, J. Model for predicting ultrasonic pulse-echo probability of detection. *NDT E. Int.* **1993**, *26*, 19–29.
13. Jacovitti, G.; Scarano, G. Discrete time techniques for time delay estimation. *IEEE Trans. Signal Process.* **1993**, *41*, 525–533.
14. International Electrotechnical Commission. Safety of Laser Products–Part 1: Equipment Classification and Requirements. Technical report, IEC-60825-1, Geneva, Switzerland, 2014.
15. Hiskett, P.A.; Parry, C.S.; McCarthy, A.; Buller, G.S. A photon-counting time-of-flight ranging technique developed for the avoidance of range ambiguity at gigahertz clock rates. *Opt. Express* **2008**, *16*, 13685–13698.
16. Krichel, N.J.; McCarthy, A.; Buller, G.S. Resolving range ambiguity in a photon counting depth imager operating at kilometer distances. *Opt. Express* **2010**, *18*, 9192–9206.
17. Liang, Y.; Huang, J.; Ren, M.; Feng, B.; Chen, X.; Wu, E.; Wu, G.; Zeng, H. 1550-nm time-of-flight ranging system employing laser with multiple repetition rates for reducing the range ambiguity. *Opt. Express* **2014**, *22*, 4662–4670.
18. Kim, G.; Park, Y. LIDAR pulse coding for high resolution range imaging at improved refresh rate. *Opt. Express* **2016**, *24*, 23810–23828. doi:10.1364/OE.24.023810.
19. Kim, G.; Park, Y. Independent Biaxial Scanning Light Detection and Ranging System Based on Coded Laser Pulses without Idle Listening Time. *Sensors* **2018**, *18*, 2943.
20. Fersch, T.; Weigel, R.; Koelpin, A. A CDMA modulation technique for automotive time-of-flight LiDAR systems. *IEEE Sensors J.* **2017**, *17*, 3507–3516.
21. Yin, H.; Richardson, D.J. *Optical Code Division Multiple Access Communication Networks*; Springer Science & Business, 2008.
22. Ghafouri-Shiraz, H.; Karbassian, M.M. *Optical CDMA Networks: Principles, Analysis and Applications*; John Wiley & Sons: Hoboken, NJ, USA, 2012.
23. Ghassemlooy, Z.; Popoola, W.; Rajbhandari, S. *Optical wireless communications: System and channel modelling with Matlab®*; CRC Press: Boca Raton, Florida, USA, 2013.
24. Yang, G.C.; Kwong, W.C. *Prime Codes with Applications to CDMA Optical and Wireless Networks*; Artech House: Norwoord, MA, USA, 2002.
25. Kwong, W.C.; Yang, G.C. *Optical Coding Theory with Prime*; CRC Press: Boca Raton, FL, USA, 2013.
26. Aldibbiat, N.M. Optical wireless communication systems employing dual header pulse interval modulation (DH-PIM). PhD thesis, Sheffield Hallam University, 2001.
27. Kaushal, H.; Kaddoum, G. Optical communication in space: Challenges and mitigation techniques. *IEEE Commun. Surv. Tutor.* **2017**, *19*, 57–96.
28. Zeng, Z.; Fu, S.; Zhang, H.; Dong, Y.; Cheng, J. A survey of underwater optical wireless communications. *IEEE Commun. Surv. Tutor.* **2017**, *19*, 204–238.
29. Park, H. Coded modulation and equalization for wireless infrared communications. PhD thesis, School of Electrical and Computer Engineering, Georgia Institute of Technology, 1997.
30. Kaluarachchi, E.D. Digital pulse interval modulation for optical communication systems. PhD thesis, Sheffield Hallam University, 1997.
31. Sugiyama, H.; Nosu, K. MPPM: A method for improving the band-utilization efficiency in optical PPM. *J. Light. Technol.* **1989**, *7*, 465–472.
32. Atkin, G.E.; Fung, K.S. Coded multipulse modulation in optical communication systems. *IEEE Trans. Commun.* **1994**, *42*, 574–582.

33. Park, H.; Barry, J.R. Modulation analysis for wireless infrared communications. Communications, 1995. ICC'95 seattle,'Gateway to Globalization', 1995 IEEE International Conference on. IEEE, 1995, Vol. 2, pp. 1182–1186.
34. Park, H. Performance bound on multiple-pulse position modulation. *Opt. Rev.* **2003**, *10*, 131–132.
35. Xu, F.; Khalighi, M.A.; Bourennane, S. Coded PPM and multipulse PPM and iterative detection for free-space optical links. *IEEE J. Opt. Commun. Netw.* **2009**, *1*, 404–415.
36. Chen, L. An enhanced pulse position modulation (PPM) in ultra-wideband (UWB) systems. Master's thesis, University of Northern Iowa, 2014.
37. Ghassemlooy, Z.; Hayes, A.; Seed, N.; Kaluarachchi, E. Digital pulse interval modulation for optical communications. *IEEE Commun. Mag* **1998**, *36*, 95–99.
38. Shiu, D.s.; Kahn, J.M. Differential pulse-position modulation for power-efficient optical communication. *IEEE trans. commun.* **1999**, *47*, 1201–1210.
39. Park, H.; Barry, J.R. Performance of multiple pulse position modulation on multipath channels. *IEE Proc.-Optoelectron.* **1996**, *143*, 360–364.
40. Jiang, Y.; Tao, K.; Song, Y.; Fu, S. Packet error rate analysis of OOK, DPIM, and PPM modulation schemes for ground-to-satellite laser uplink communications. *Appl. Optics* **2014**, *53*, 1268–1273.
41. Shinwasusin, E.a.; Charoenlarpnopparut, C.; Suksompong, P.; Taparugssanagorn, A. Modulation performance for visible light communications. Information and Communication Technology for Embedded Systems (IC-ICTES), 2015 6th International Conference of. IEEE, 2015, pp. 1–4.
42. Salehi, J.A. Code division multiple-access techniques in optical fiber networks. I. Fundamental principles. *IEEE Transactions on communications* **1989**, *37*, 824–833.
43. Salehi, J.A.; Brackett, C.A. Code division multiple-access techniques in optical fiber networks. II. Systems performance analysis. *IEEE Transactions on Communications* **1989**, *37*, 834–842.
44. Mashhadi, S.; Salehi, J.A. Code-division multiple-access techniques in optical fiber networks-Part III: Optical AND logic gate receiver structure with generalized optical orthogonal codes. *IEEE Trans. Commun.* **2006**, *54*, 1457–1468.
45. Zhang, J.G.; Kwong, W.C.; Sharma, A. Effective design of optical fiber code-division multiple access networks using the modified prime codes and optical processing. Communication Technology Proceedings, 2000. WCC-ICCT 2000. International Conference on. IEEE, 2000, Vol. 1, pp. 392–397.
46. Azizoglu, M.; Salehi, J.A.; Li, Y. Optical CDMA via temporal codes. *IEEE Trans. Commun.* **1992**, *40*, 1162–1170.
47. Walker, E.L. A theoretical analysis of the performance of code division multiple access communications over multimode optical fiber channels-part I: transmission and detection. *IEEE J. Sel. Areas Commun.* **1994**, *12*, 751–761.
48. Yang, G.C.; Kwong, W.C. Performance analysis of optical CDMA with prime codes. *Electron. Lett.* **1995**, *31*, 569–570.
49. Zhang, J.G.; Kwong, W. Effective design of optical code-division multiple access networks by using the modified prime code. *Electron. Lett.* **1997**, *33*, 229–230.
50. Glesk, I.; Huang, Y.K.; Brès, C.S.; Prucnal, P.R. Design and demonstration of a novel optical CDMA platform for use in avionics applications. *Opt. Commun.* **2007**, *271*, 65–70.
51. Qian, J.; Karbassian, M.M.; Ghafouri-Shiraz, H. Energy-efficient high-capacity optical CDMA networks by low-weight large code-set MPC. *J. Light. Technol.* **2012**, *30*, 2876–2883.
52. Karbassian, M.M.; Küppers, F. Enhancing spectral efficiency and capacity in synchronous OCDMA by transposed-MPC. *Opt Switch. Netw.* **2012**, *9*, 130–137.
53. Sabatini, R.; Richardson, M.A. Airborne Laser Systems Testing and Analysis. Report, NATO Science and Technology Organization, Brussels, Belgium, 2010.
54. Abdullah, Q.; Maune, D.; Smith, D.C.; Heidemann, H.K. New Standard for New Era: Overview of the 2015 ASPRS Positional Accuracy Standards for Digital Geospatial Data. *Programmetric Engineering & Remote Sensing* **2015**, *81*, 173–176.
55. American Society for Photogrammetry and Remote Sensing. ASPRS Positional Accuracy Standards for Digital Geospatial Data. *Photogramm. Eng. Remote Sensing* **2015**, *81*, A1–A26.